Journal of the Optical Society of America B
OPTICAL PHYSICS

Fast vertical mode expansion method for the simulation of extraordinary terahertz field enhancement in an annular nanogap

Zhen Hu,[1] Junshan Lin,[2,*] Ya Yan Lu,[3] and Sang-Hyun Oh[4]

[1]Department of Mathematics, Hohai University, Nanjing, Jiangsu, China
[2]Department of Mathematics and Statistics, Auburn University, Auburn, Alabama 36849, USA
[3]Department of Mathematics, City University of Hong Kong, Kowloon, Hong Kong
[4]Department of Electrical and Computer Engineering, University of Minnesota, Minneapolis, Minnesota 55455, USA
*Corresponding author: jzl0097@auburn.edu

Received 22 August 2017; revised 31 October 2017; accepted 7 November 2017; posted 8 November 2017 (Doc. ID 305366); published 4 December 2017

This paper is concerned with electromagnetic wave scattering of an annular nanogap in the terahertz regime. We present an efficient vertical mode expansion method (VMEM) to solve the scattering problem, and study the extraordinary optical transmission and field enhancement for the nanostructure with various configurations. The VMEM expands the electromagnetic field in and outside the nanogap along the invariant direction by the one-dimensional modes, where the expansion coefficients satisfy scalar two-dimensional Helmholtz equations on the cross-sectional plane. The continuity conditions of electromagnetic fields on the vertical boundaries of neighboring regions are then employed to establish the linear system for the unknown coefficients. Based on the numerical simulations, we investigate the field enhancement in the nanogap. In particular, we investigate the nanostructure with a series of gap sizes and push the gap width limit to 1 nm in the numerical simulation. The normal and oblique incidence cases and the transverse electric (TE) and transverse magnetic (TM) polarization cases are considered.

OCIS codes: (290.0290) Scattering; (310.6628) Subwavelength structures, nanostructures; (250.5403) Plasmonics; (050.1755) Computational electromagnetic methods.

https://doi.org/10.1364/JOSAB.35.000030

1. INTRODUCTION

Motivated by significant applications in sensing, spectroscopy, and nano-optics, the effect of extraordinary optical transmission through subwavelength apertures has been investigated extensively since Ebbesen's seminal paper [1]. Various subwavelenth structures have been developed to achieve strongly confined electromagnetic field near the apertures. These include metallic films perforated with periodic arrays of subwavelenth holes or slits, single nano-sized hole or slit, and others. We refer the readers to the review papers [2,3] and references therein for detailed discussions.

In this paper, we numerically study the enhancement of terahertz (THz) wave inside a single annular nanometer-wide gap that is perforated in a gold film. The terahertz frequency domain is an emerging technological frontier with many potential applications in sensing, spectroscopy, and materials characterization [4,5]. New techniques have been developed to confine and manipulate terahertz waves using metallic nanostructures (see, for example, [6–8]). Previously, researchers have shown that there are extraordinary optical transmission and enormously enhanced electric field for small annular gaps, and the field enhancement intensity in the gap keeps increasing with a decreasing gap width [9–14]. Theoretical and experimental studies of the plasmon dispersion in annular gaps have also been reported in [15–18]. Here we present numerical simulations for such extraordinary optical transmission and field enhancement. In addition, we investigate the resonant phenomenon and field enhancement in various configurations. These include scattering with normal and oblique incident waves, TE and TM polarizations, and nanostructures with varying metal film thicknesses and gap sizes. If the gold film is approximately viewed as perfectly electrical conductor, the underlying structure becomes a coaxial waveguide [19]. We model the gold film as a dispersive and lossy material. In the numerical simulation, we also push the gap size to the limit of 1 nm in order to gain strongly localized wave field. This regime was not extensively explored previously, but with recent advances in nanofabrication, it is now possible to make THz-resonant gaps that are as narrow as 1 nm [7,8].

The numerical modeling of the scattering problem requires solving the full three-dimensional Maxwell's equations in a multiscale medium, which is challenging due to the smallness of the gap size. Especially, there is extreme scale difference between the wavelength and the gap size. The former ranges from a few hundred microns to a few millimeters in the terahertz regime, whereas the latter has only a few nanometers. Standard numerical approaches such as the finite-difference time-domain (FDTD) method and the finite element method (FEM) would require huge computational resources, since it is necessary to impose tiny grid size in order to resolve the wave fields inside the narrow gap. Here we employ an efficient vertical mode expansion method (VMEM) to analyze the electromagnetic field for the annular gap structure. The VMEM method was recently developed in [20–22] and has also been applied to analyze the electromagnetic field for the bull's eye structures [23]. In contrast to the usual mode matching method, the VMEM method divides the geometry of the problem into several regions, which are infinite along the vertical z direction. By expanding the wave field in each region and matching the tangential field components on the boundaries of these regions, a small linear system associated with the expansion coefficients is solved. The method is well suited for problems with a continuous rotational symmetry, such as the annular gap considered here.

The rest of the paper is organized as follows. We introduce the geometry of the nanostructure and formulate the scattering problem in Section 2. In Section 3, we outline the vertical mode expansion method (VMEM) for solving the scattering problem. Various numerical results are presented in Section 4 to investigate the resonant phenomenon and the field enhancement in the nanogap. We end the paper by some concluding remarks in Section 5.

2. PROBLEM FORMULATION

A thin gold film with a thickness of d is deposited on the glass substrate and extends to infinity on the xy-plane. A coaxial waveguide is then perforated in the gold film such that it forms an annular gap on the xy plane and is invariant along the z direction (see Fig. 1). For simplicity of modeling, we assume that the substrate is semi-infinite and occupies the domain

$$D_+ := \{(x, y, z) | z > d\}.$$

The gold film occupies the domain

$$D_d := \{(x, y, z) | 0 < z < d\}.$$

Denote the outer and inner radius of the annulus aperture by R_1 and R_0, respectively; then the gap width $w = R_1 - R_0$. The coaxial waveguide is a cylinder given by

$$D_w := \{(x, y, z) | (x, y) \in B_{R_1} \backslash B_{R_0}, 0 < z < d\},$$

where B_{R_0} and B_{R_1} are discs with radii of R_0 and R_1, respectively. We consider the gap size w in the nanometer regime so as to maximize the enhancement of the wave field when it passes through the gap. The fabrication technique employed to produce such a tiny gap, called atomic layer lithography, fills the gap with a metal oxide film such as alumina [8,12,14,24].

We assume that the material is nonmagnetic by setting the magnetic permeability $\mu = \mu_0$, wherein μ_0 is the magnetic permeability of the vacuum. The relative permittivity of the gold film is evaluated by the Drude model (cf. [25]) such that

$$\varepsilon_r(\omega) = 1 - \frac{w_p^2}{\omega(\omega + i\gamma)}.$$

Here the plasma frequency $w_p = 1.37 \times 10^4$ Tera-Radian/s and $\gamma = 40.7$ Tera-Radian/s. The refractive indices of the glass substrate and the alumina that fill the annular nanogap are set as $n_{SiO_2} = 1.95$ and $n_{Al_2O_3} = 2.12$, respectively [26]. Thus, the relative permittivity values in the domains D_+ and D_w are $\varepsilon_r = 3.80$ and $\varepsilon_r = 4.49$, respectively.

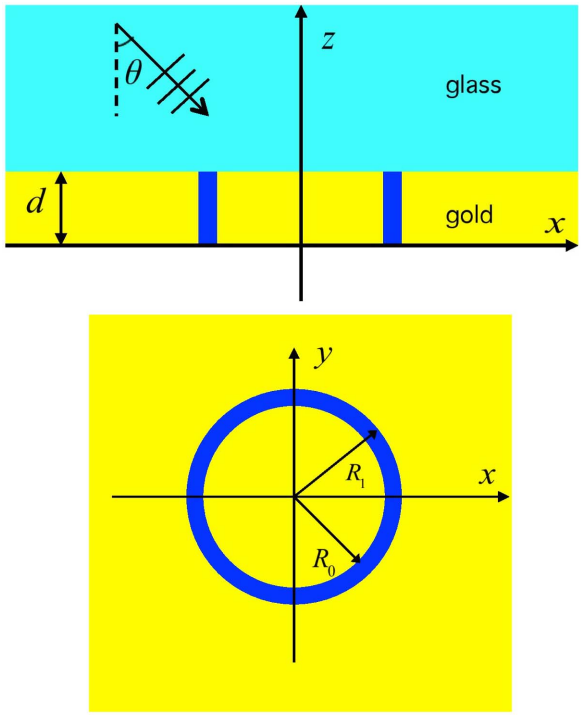

Fig. 1. Side view (top) and top view (bottom) of the nanostructure. Size of the annular gap $w = R_1 - R_0$.

Consider a time-harmonic terahertz (THz) wave $\{\mathbf{E}^i, \mathbf{H}^i\}$ (with $e^{-i\omega t}$ time dependence) that impinges on the metallic nanostructure from the top. In the absence of the annular gap, the incident plane wave gives rise to a reflected wave and a transmitted wave above and below the gold film, respectively. With the annular gap, a scattered wave $\{\hat{\mathbf{E}}^s, \hat{\mathbf{H}}^s\}$ is present, and it propagates in all directions. The total electrical field $\hat{\mathbf{E}}$ and the magnetic field $\hat{\mathbf{H}}$ after the scattering are governed by the following Maxwell's equations in the frequency domain:

$$\nabla \times \hat{\mathbf{E}} = i\omega\mu\hat{\mathbf{H}}, \qquad \nabla \times \hat{\mathbf{H}} = -i\omega\varepsilon\hat{\mathbf{E}} \quad \text{in} \quad \mathbb{R}^3.$$

Let us define $\mathbf{E} = \sqrt{\varepsilon_0}\hat{\mathbf{E}}$ and $\mathbf{H} = \sqrt{\mu_0}\hat{\mathbf{E}}$, and then rewrite the Maxwell's equations in terms of relative physical parameters as

$$\nabla \times \mathbf{E} = ik_0\mathbf{H}, \qquad \nabla \times \mathbf{H} = -ik_0\varepsilon_r\mathbf{E} \quad \text{in} \quad \mathbb{R}^3,$$

where k_0 is the free space wavenumber. In addition, the scattered field $\{\hat{\mathbf{E}}^s, \hat{\mathbf{H}}^s\}$ satisfies the outgoing radiation condition.

3. VERTICAL MODE EXPANSION METHOD

We employ the VMEM method to solve the scattering problem numerically. In contrast to the traditional horizontal mode matching method, the key idea of the VMEM method is to expand the electromagnetic field in and outside the nanogap along the invariant z direction by the one-dimensional modes, where the expansion coefficients satisfy scalar two-dimensional Helmholtz equations on the xy-plane. The matching of electromagnetic fields is then imposed on vertical boundaries of the regions in and outside the nanogap. The method is well suited for problems with a continuous rotational symmetry, and it has been applied to the modeling of electromagnetic scattering of various nanostructures, including a circular hole, bull's eye, photonic crystal slabs, and others [20–23]. Here we apply the method to optical scattering by the annular gap, which also attains a rotational symmetry. In what follows we outline the method and refer the reader to [20] for detailed derivations.

First, the whole $\mathbb{R}^3$ is decomposed into three domains, D_0, D_1, and D_2, which are infinite along the vertical z direction as shown in Fig. 2. We adopt the cylinder coordinate where $x = r\cos\varphi$ and $y = r\sin\varphi$; then

$$D_0 := \{(r,\varphi,z)|r < R_0, 0 \le \varphi < 2\pi, -\infty < z < \infty\},$$

$$D_1 := \{(r,\varphi,z)|R_0 < r < R_1, 0 \le \varphi < 2\pi, -\infty < z < \infty\},$$

$$D_2 := \{(r,\varphi,z)|r > R_1, 0 \le \varphi < 2\pi, -\infty < z < \infty\}.$$

The cross sections of the domains D_0, D_1, and D_2 are denoted by S_0, S_1, and S_2, respectively. In each domain D_ℓ, the permittivity $\varepsilon_r^{(\ell)}$ is a piecewise constant along the z direction and is invariant on the cross section S_ℓ. As such, the electromagnetic field can be written down as the sum of the vertical modes, which are 1D solutions along the z direction.

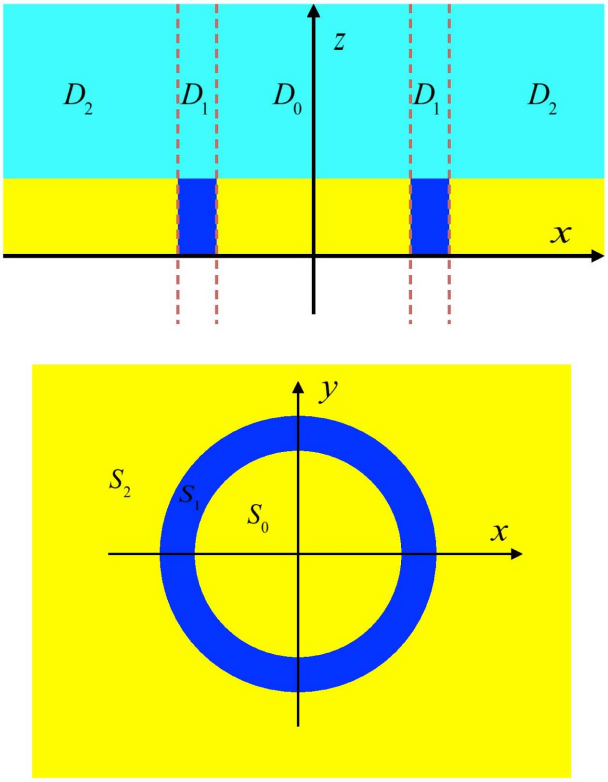

Fig. 2. Side view (top) and top view (bottom) of decomposed domains D_0, D_1, and D_2.

For the transverse electric (TE) wave with $E_z^s = 0$ and $H_z^s \neq 0$, the scattered field H_z^s in $D_\ell(\ell = 0, 1, 2)$ can be expressed as

$$H_z^s = \sum_{j=1}^{\infty} [\eta_j^{(\ell,e)}]^2 V_j^{(\ell,e)}(x,y)\phi_j^{(\ell,e)}(z), \tag{1}$$

where $\eta_j^{(\ell,e)}$ and $\phi_j^{(\ell,e)}$ are the eigenvalues and the corresponding eigenfunctions of the following 1D problem:

$$\frac{d^2\phi_j^{(\ell,e)}}{dz^2} + k_0^2\varepsilon_r^{(\ell)}\phi_j^{(\ell,e)} = [\eta_j^{(\ell,e)}]^2\phi_j^{(\ell,e)}, \qquad -\infty < z < \infty. \tag{2}$$

Here we use the superscript e to denote the TE wave. Then from the Maxwell's equations, it follows that $V_j^{(\ell,e)}$ satisfies

$$\Delta V_j^{(\ell,e)} + [\eta_j^{(\ell,e)}]^2 V_j^{(\ell,e)} = 0 \quad \text{in } S_\ell, \tag{3}$$

where $\Delta = \partial_x^2 + \partial_y^2$ denotes the Laplace operator. Similarly, for the transverse magnetic (TM) wave with $H_z^s = 0$ and $E_z^s \neq 0$, we express E_z^s in $D_\ell(\ell = 0, 1, 2)$ as

$$E_z^s = \frac{1}{\varepsilon_r^{(\ell)}} \sum_{j=1}^{\infty} [\eta_j^{(\ell,h)}]^2 V_j^{(\ell,h)}(x,y)\phi_j^{(\ell,h)}(z), \tag{4}$$

where $\eta_j^{(\ell,h)}$ and $\phi_j^{(\ell,h)}$ are the eigenvalues and eigenfunctions of the 1D problem:

$$\varepsilon_r^{(\ell)}\frac{d}{dz}\left(\frac{1}{\varepsilon_r^{(\ell)}}\frac{d\phi_j^{(\ell,h)}}{dz}\right) + k_0^2\varepsilon_r^{(\ell)}\phi_j^{(\ell,h)} = [\eta_j^{(\ell,h)}]^2\phi_j^{(\ell,h)}, \quad -\infty < z < \infty, \tag{5}$$

and $V_j^{(\ell,h)}$ satisfies

$$\Delta V_j^{(\ell,h)} + [\eta_j^{(\ell,h)}]^2 V_j^{(\ell,h)} = 0 \quad \text{in } S_\ell. \tag{6}$$

To obtain the eigenvalues and eigenfunctions $\eta_j^{(\ell,p)}$ and $\phi_j^{(\ell,p)}$ $(p = e, h)$, the infinite domain of the 1D problems Eqs. (2) and (5) is truncated to a finite interval (z_b, z_t). The perfectly matched layers (PMLs) are applied near the two endpoints with zero Dirichlet boundary conditions [27]. Using the rotational symmetry of the problem, the solution $V_j^{(\ell,p)}$ $(p = e, h)$ can be expressed as the sum of Bessel functions. More precisely,

$$V_j^{(0,p)} = \sum_{m=-\infty}^{\infty} b_{j,m}^{(0,p)} \frac{J_m(\eta_j^{(0,p)}r)}{J_m(\eta_j^{(0,p)}R_0)} e^{im\varphi} \quad \text{in } S_0, \tag{7}$$

$$V_j^{(1,p)} = \sum_{m=-\infty}^{\infty} \left[a_{j,m}^{(1,p)} \frac{H_m^{(1)}(\eta_j^{(1,p)}r)}{H_m^{(1)}(\eta_j^{(1,p)}R_0)} + b_{j,m}^{(1,p)} \frac{H_m^{(2)}(\eta_j^{(1,p)}r)}{H_m^{(2)}(\eta_j^{(1,p)}R_1)}\right] e^{im\varphi} \quad \text{in } S_1, \tag{8}$$

$$V_j^{(2,p)} = \sum_{m=-\infty}^{\infty} a_{j,m}^{(2,p)} \frac{H_m^{(1)}(\eta_j^{(2,p)}r)}{H_m^{(1)}(\eta_j^{(2,p)}R_1)} e^{im\varphi} \quad \text{in } S_2. \tag{9}$$

Here J_m is the mth order Bessel function of the first kind, and $H_m^{(1)}$ and $H_m^{(2)}$ are the mth order Hankel functions of first and second kinds.

Let $\{\mathbf{E}^{(\ell)}, \mathbf{H}^{(\ell)}\}$ be the total field associated with the layered medium for the incident wave $\{\mathbf{E}^i, \mathbf{H}^i\}$, where the permittivity $\varepsilon_r(z) = \varepsilon_r^{(\ell)}(z)$. In light of Eqs. (1) and (4), it follows that, in each region, the total field with the annular gap is given by

$$H_z = H_z^{(\ell)} + \sum_{j=1}^{\infty} [\eta_j^{(\ell,e)}]^2 V_j^{(\ell,e)} \phi_j^{(\ell,e)}, \tag{10}$$

$$E_z = E_z^{(\ell)} + \frac{1}{\varepsilon_r^{(\ell)}} \sum_{j=1}^{\infty} [\eta_j^{(\ell,h)}]^2 V_j^{(\ell,h)} \phi_j^{(\ell,h)}, \tag{11}$$

$$H_\tau = H_\tau^{(\ell)} + \sum_{j=1}^{\infty} \frac{\partial V_j^{(\ell,e)}}{\partial \tau} \frac{d\phi_j^{(\ell,e)}}{dz} + ik_0 \sum_{j=1}^{\infty} \frac{\partial V_j^{(\ell,h)}}{\partial \nu} \phi_j^{(\ell,h)}, \tag{12}$$

$$E_\tau = E_\tau^{(\ell)} + \frac{1}{\varepsilon_r^{(\ell)}} \sum_{j=1}^{\infty} \frac{\partial V_j^{(\ell,h)}}{\partial \tau} \frac{d\phi_j^{(\ell,h)}}{dz} - ik_0 \sum_{j=1}^{\infty} \frac{\partial V_j^{(\ell,e)}}{\partial \nu} \phi_j^{(\ell,e)}. \tag{13}$$

In the above, $\nu = (\nu_x, \nu_y)$ and $\tau = (-\nu_y, \nu_x)$ denote the unit outward normal vector and tangential vector, respectively, along the boundaries ∂D_ℓ, H_τ, and E_τ, which are the tangential components in the τ direction.

By substituting Eqs. (7)–(9) into the expansions Eqs. (10)–(13) and imposing the continuity conditions for the electromagnetic fields over the discrete points z_j ($j = 1, 2, 3, \ldots, N$) and for $r = R_0$ and R_1, we collect the Fourier coefficients for each m and obtain a linear system

$$\mathbf{A}_m \mathbf{x}_m = \mathbf{c}_m. \tag{14}$$

$\mathbf{A}_m$ is a $8N \times 8N$ matrix, and the unknown vector

$$\mathbf{x}_m = \begin{bmatrix} \mathbf{b}_m^{(0,e)} \\ \mathbf{b}_m^{(0,h)} \\ \mathbf{a}_m^{(1,e)} \\ \mathbf{a}_m^{(1,h)} \\ \mathbf{b}_m^{(1,e)} \\ \mathbf{b}_m^{(1,h)} \\ \mathbf{a}_m^{(2,e)} \\ \mathbf{a}_m^{(2,h)} \end{bmatrix}, \qquad \mathbf{a}_m^{(\ell,p)} = \begin{bmatrix} a_{1,m}^{(\ell,p)} \\ a_{2,m}^{(\ell,p)} \\ \vdots \\ a_{N,m}^{(\ell,p)} \end{bmatrix}, \qquad \mathbf{b}_m^{(\ell,p)} = \begin{bmatrix} b_{1,m}^{(\ell,p)} \\ b_{2,m}^{(\ell,p)} \\ \vdots \\ b_{N,m}^{(\ell,p)} \end{bmatrix}.$$

The vector $\mathbf{c}_m$ is given by

$$\mathbf{c}_m = [\,\mathbf{c}_m^{(1,1)} \quad \mathbf{c}_m^{(1,2)} \quad \mathbf{c}_m^{(1,3)} \quad \mathbf{c}_m^{(1,4)} \quad \mathbf{c}_m^{(2,1)} \quad \mathbf{c}_m^{(2,2)} \quad \mathbf{c}_m^{(2,3)} \quad \mathbf{c}_m^{(2,4)}\,]^T,$$

where the entries of sub-columns $\mathbf{c}_m^{(1,1)}$ and $\mathbf{c}_m^{(2,1)}$ are the Fourier coefficients of the expansions

$$H_z^{(1)}(R_0, \varphi, z_j) - H_z^{(0)}(R_0, \varphi, z_j) = \sum_{m=-\infty}^{\infty} c_{j,m}^{(1,1)} e^{im\varphi},$$

$$H_z^{(2)}(R_1, \varphi, z_j) - H_z^{(1)}(R_1, \varphi, z_j) = \sum_{m=-\infty}^{\infty} c_{j,m}^{(2,1)} e^{im\varphi}.$$

Similarly, the entries of sub-columns $\mathbf{c}_m^{(\ell,2)}$, $\mathbf{c}_m^{(\ell,3)}$, and $\mathbf{c}_m^{(\ell,4)}$ ($\ell = 1, 2$) are defined as the Fourier coefficients of the expansions for $E_z^{(\ell)} - E_z^{(\ell-1)}$, $H_\tau^{(\ell)} - H_\tau^{(\ell-1)}$, and $E_\tau^{(\ell)} - E_\tau^{(\ell-1)}$, respectively. By solving the linear system Eq. (14), we obtain all the expansion coefficients for the total electromagnetic field.

4. RESONANCES AND FIELD ENHANCEMENT INSIDE THE NANOGAP

We consider the configuration where the gold film has a thickness $d = 150$ nm, and the inner radius of the annulus is $R_0 = 50$ μm. The frequency of the incident wave is in the THz regime so that strong resonance will be observed. We consider both the normal incidence and the oblique incidence and investigate the enhanced transmission and field enhancement at resonant frequencies for various gap sizes that range from 1 nm to 50 nm.

In the numerical computation, the number of discretization points N along the z axis are chosen such that the oscillatory behavior of the electromagnetic waves is accurately resolved inside and outside the metallic slab. Note that N depends on the wavelength and the thickness of the metallic slab, while it does not strongly depends on the radii of the annulus and the gap size. Since on the xy-plane, the modes are expressed analytically in terms of Bessel functions as shown in Eqs. (7)–(9). We also point out that the linear system Eq. (14) can be solved efficiently by direct solvers (such as the LU decomposition), since the size of the matrix is relatively small.

A. Normal Incidence

We consider that the normal incident wave and the electric field have only a nonzero x component such that

$$\mathbf{E}^i = \begin{bmatrix} E_x^i \\ 0 \\ 0 \end{bmatrix}.$$

Figure 3 demonstrates the normalized transmission T for various gap sizes that range from 1 nm to 50 nm. Here the normalized transmission T is defined by

$$T = \frac{P^{\text{extra}}}{P^{\text{inc}}}, \tag{15}$$

where P^{extra} is the extra transmitted power and P^{inc} is the power of normal incident wave over the gap aperture. We define the extra transmitted power by

$$P^{\text{extra}} = -\int_{\mathbb{R}^2} (\mathbf{S}_z - \mathbf{S}_z^{(0)}) \mathrm{d}x\mathrm{d}y,$$

for any $z < 0$. In the above, $\mathbf{S}_z$ and $\mathbf{S}_z^{(0)}$ are the z component of the Poynting vector when the gap is present and not, respectively. Notice that P^{extra} is independent of z. In the computation, we reduce the above integral on $\mathbb{R}^2$ to line integrals on circles with radii R_0 and R_1.

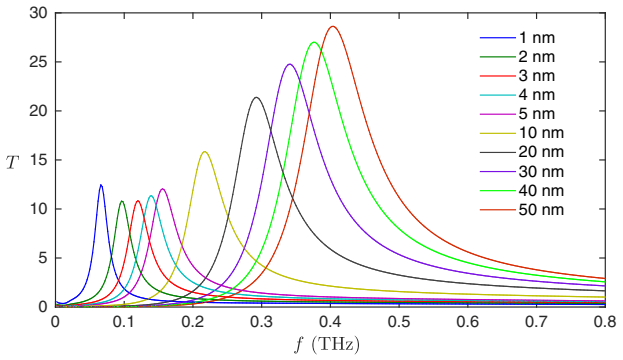

Fig. 3. Normalized transmission T for various frequencies f and different gap sizes w.

First, it is observed that, for a specified gap width w, the transmission T exhibits a peak in the terahertz regime. At the peak, the value of T exceeds 10 for all gap sizes. In particular, T is over 25 at the frequency $f = 0.404$ THz (or at the wavelength $\lambda = 0.743$ mm) when the gap width is 50 nm. That is, the transmission with the annular gap is more than 25 times higher compared to the power incident on the open area of the gap. Such peak values are related to the Fabry–Perot type resonances that propagate along the length of the coaxial waveguide and are believed to occur near the cutoff frequency for the TE_{11} waveguide mode [14,15]. To investigate the field enhancement at the resonant frequencies, we consider the gap width $w = 5$ nm and plot $|E_x|$, the magnitude for the x component of the electric field, at the resonant frequency $f = 0.156$ THz in Figs. 4 and 5. Both the cross-sectional plots on the xy and xz plane are shown, and it is seen that an enhancement order over 5000 is achieved inside the annular gap for the electric field amplitude. In addition, as observed from Fig. 4, the electric field has a $\cos\varphi$ dependence, which also verifies the excitation of the TE_{11} mode in the waveguide.

It is also seen from Fig. 3 that the peak of the transmission T (or the resonant frequency) shifts to lower frequencies as the gap size w decreases. Figure 6 plots the resonant frequencies as w increases from 1 nm to 50 nm. A very interesting feature of the resonances for the annular nanogap is the significant shift of the resonant frequency with a tiny change of the gap size. For instance, as w decreases from 5 nm to 1 nm, the resonant frequency shifts from 0.156 THz to 0.06 THz. It is known that the cutoff wavelength of a perfect electrical conducting (PEC) coaxial waveguide is given by $n_{Al_2O_3} \cdot \pi(R_0 + R_1)$ [15]. Hence, the PEC theory is not sufficient to explain the significant shift of the resonant frequency. On the other hand, it is noted that the cutoff wavelength for the coaxial waveguides made with a real metal differs dramatically from the PEC approximation, especially as the gap size is reduced, and it is believed the cylindrical surface plasmons play an important role in the resonant frequency shift [11,15].

To demonstrate the enormous field enhancement as the gap size decreases, we calculate the enhancement factor Q at the resonant frequencies, where Q is defined as the ratio between the amplitude of the total field and the incident field given by

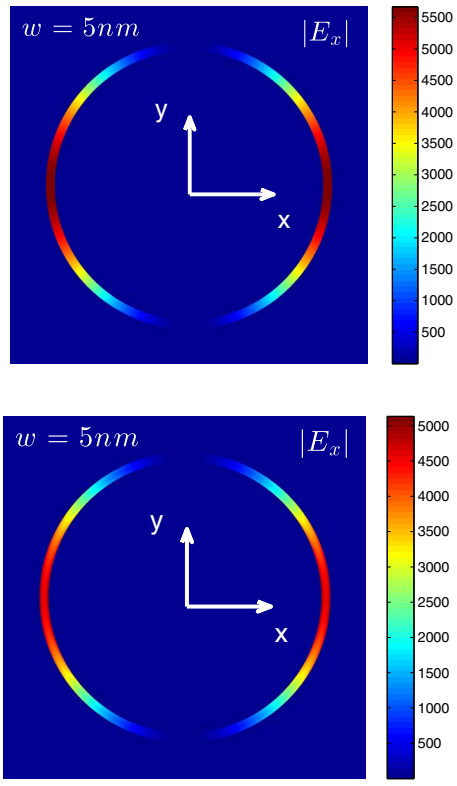

Fig. 4. Cross-sectional plot of $|E_x|$ on the xy plane at the resonant frequency $f = 0.156$ THz: at $z = 75$ nm (top) and at $z = 150.4$ nm (bottom). Gap width is $w = 5$ nm. Radial variable r is stretched to enlarge the annular gap in the figures.

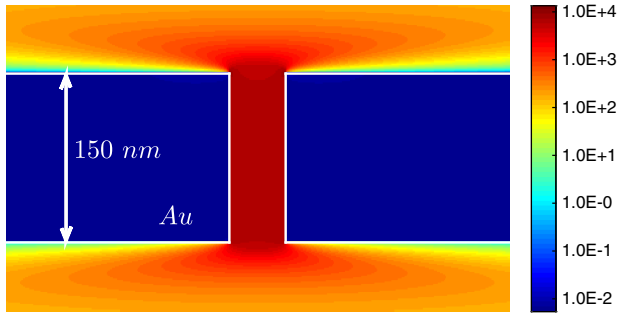

Fig. 5. Cross-sectional plot of $|E_x|$ at the resonant frequency $f = 0.156$ THz on the xz plane when $y = 0$. Gap width is $w = 5$ nm.

$$Q = \frac{|\mathbf{E}|}{|\mathbf{E}^i|}.$$

The enhancement factor Q in the middle of the coaxial waveguide, namely at the location $(x, y, z) = (R_0 + w/2, 0, d/2)$, is plotted in Fig. 7. We see that the enhancement factor exceeds 10,000 if the gap size is sufficiently small. It should be pointed out that the nonlocal electrodynamic effects in such small gaps, which may place an upper bound on the field enhancement, is not taken into account in the physical model considered here [28].

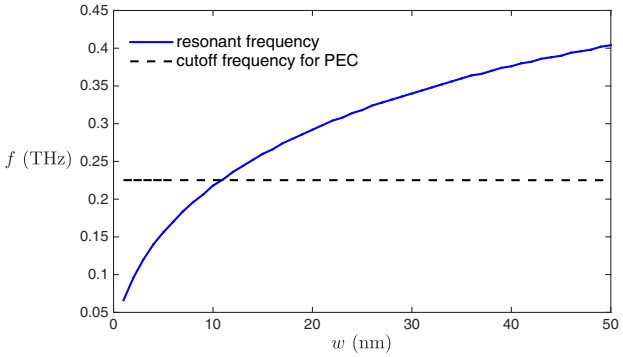

Fig. 6. Resonant frequencies for different gap sizes w. Note that the resonance frequency shifts from 0.156 THz to 0.06 THz as the gap width w decreases from 5 nm to 1 nm. For comparison, cutoff frequencies for the PEC coaxial waveguide are also shown.

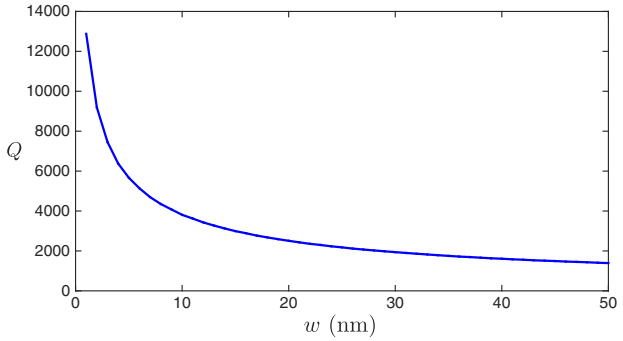

Fig. 7. Enhancement factor Q evaluated at the location $(x, y, z) = (R_0 + w/2, 0, d/2)$ for different gap sizes w.

Finally, we calculate the transmission T for several different metal film thicknesses when gap width $w = 5$ nm and then plot T values in Fig. 8. It is observed that the resonant frequency only shifts slightly as the thickness d increases from 150 nm to 300 nm. This may be because the resonant wavelength of the FP0 mode in the coaxial waveguide is mostly determined by its cutoff frequency and has a propagation constant that is not heavily dependent on the length of the waveguide [14,29]. Furthermore, we see that the transmission T increases with a decreasing thickness d.

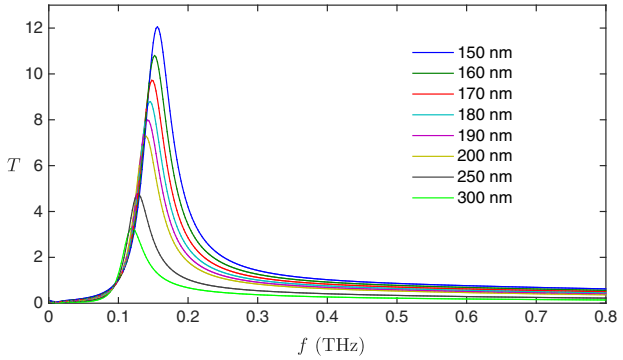

Fig. 8. Normalized transmission T for various frequencies f and different metal thicknesses d. Gap width is $w = 5$ nm.

B. Oblique Incidence

Let us assume that the incident wave vector is in the xz plane, and it forms an angle of θ with the z axis as shown in Fig. 1. The geometrical parameters of the nanostructure is the same as those in Section 4.A. We first consider the TM polarization, where

$$\mathbf{E}^i = \begin{bmatrix} E_x^i \\ 0 \\ E_z^i \end{bmatrix}, \qquad \mathbf{H}^i = \begin{bmatrix} 0 \\ H_y^i \\ 0 \end{bmatrix}.$$

For the incident angle $\theta = 15°$, the normalized transmission T with various gap sizes is shown in Fig. 9. As before, here T is defined as

$$T = \frac{P^{\text{extra}}}{P^{\text{inc}}}, \tag{16}$$

where P^{extra} is the extra transmitted power and P^{inc} is the power of normal incident wave on the gap aperture. We keep the denominator P^{inc} independent of the incident angle for the convenience of comparison among different incident angles. Correspondingly, the resonant frequencies for w varying from 1 nm to 50 nm are plotted in Fig. 10. We see that resonant frequencies of the oblique incidence are indistinguishable from those of normal incidence as shown in Fig. 6. This is consistent

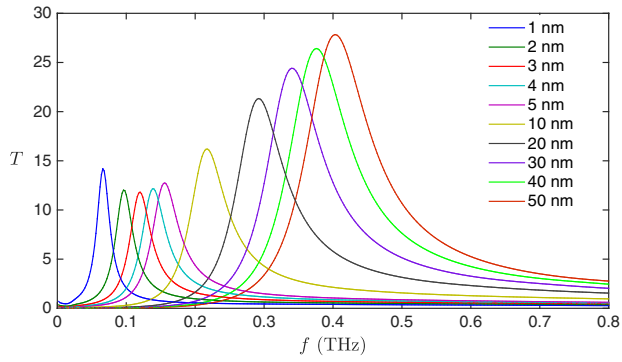

Fig. 9. Normalized transmission T for the TM polarization at various frequencies f and different gap sizes w. Incident angle is $\theta = 15°$.

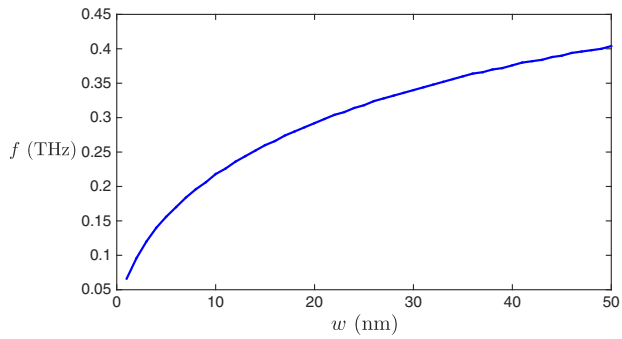

Fig. 10. Resonant frequencies for the TM polarization at different gap sizes w. The incident angle $\theta = 15°$.

with the resonance theory where the resonant frequencies are mainly dependent on the nanostructures, rather than the incident angles.

To demonstrate the field enhancement in the nanogap, we fix the incident angle $\theta = 15°$ and vary the gap sizes. The enhancement factor Q at the resonant frequencies and at the location $(x, y, z) = (R_0 + w/2, 0, d/2)$ is plotted for all gap sizes in Fig. 11. We see that enhancement factor is only slightly different from the normal incidence case.

Next we consider the TE polarized incident wave, where

$$\mathbf{E}^i = \begin{bmatrix} 0 \\ E_y^i \\ 0 \end{bmatrix}, \qquad \mathbf{H}^i = \begin{bmatrix} H_x^i \\ 0 \\ H_z^i \end{bmatrix}.$$

The normalized transmission T at the incident angle $\theta = 15°$ is plotted in Fig. 12 for all gap sizes, and the corresponding resonant frequencies are shown in Fig. 13. Very interestingly, the coincidence of Fig. 12 with Figs. 3 and 9 demonstrates the independence of the resonant frequencies on the polarization of the electromagnetic field. For completeness, we also plot the enhancement factor Q at the resonant frequencies and at the location $(x, y, z) = (R_0 + w/2, 0, d/2)$ for all gap sizes in Fig. 11. Again, we observe slight differences in the enhancement factor for two polarizations.

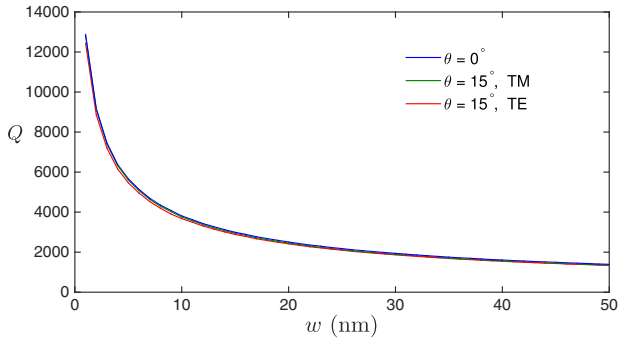

Fig. 11. Enhancement factor Q for different gap sizes w at normal and oblique incident angles. Q is evaluated at the location $(x, y, z) = (R_0 + w/2, 0, d/2)$.

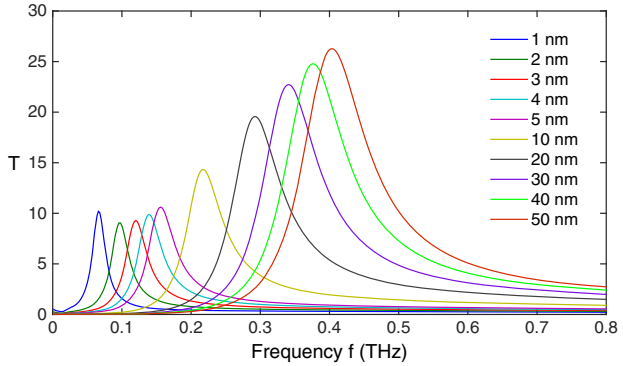

Fig. 12. Normalized transmission T for the TE polarization at various frequencies f and different gap sizes w. Incident angle is $\theta = 15°$.

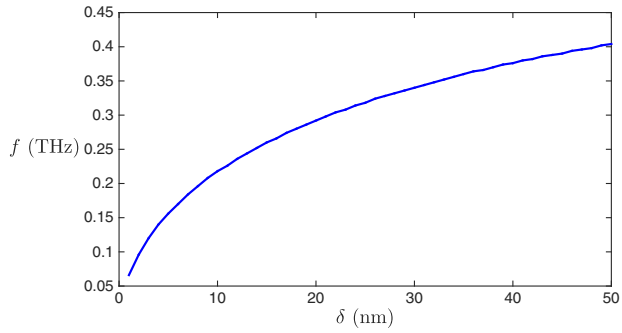

Fig. 13. Resonant frequencies for the TE polarization at different gap sizes w. Incident angle is $\theta = 15°$.

Finally, for both the TE and TM polarizations, we vary the incident angles and calculate the corresponding electric field at the location $(x, y, z) = (R_0 + w/2, 0, d/2)$ at the resonant frequencies. The magnitude of the electric field is shown in Fig. 14 when the gap width $w = 5$ nm. It is seen that the electric field enhancement varies slowly for $0 < \theta < 25°$.

C. Comparison with the Hybrid Discontinuous Galerkin Method

In this section, we compare the numerical results obtained from the VMEM with the simulations for a periodic array of coaxial apertures as presented in [12]. In [12], the field enhancement for an annular nanogap array, with a 32 μm diameter and a 50 μm array periodicity and perforated in the metal film with a 150 nm thickness, is investigated experimentally and numerically. The numerical simulation is carried out by the hybrid

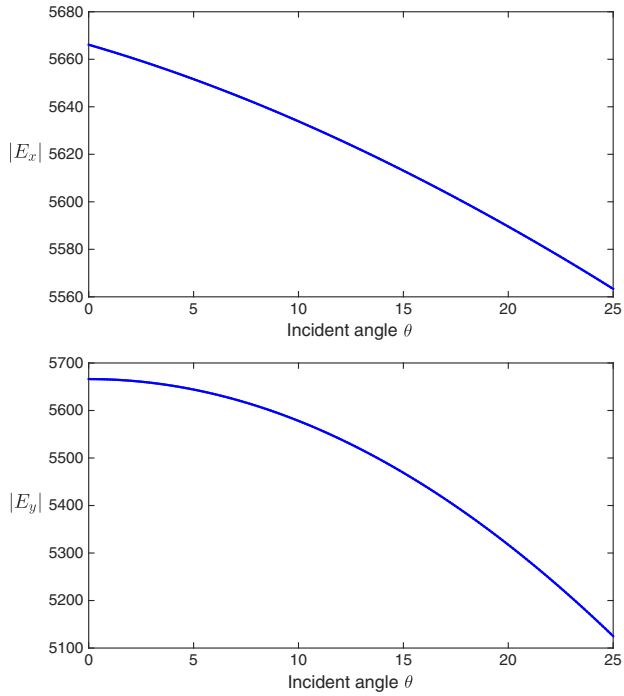

Fig. 14. $|E_x|$ for the TM polarization (top) and $|E_y|$ for the TE polarization (bottom) at the location $(x, y, z) = (R_0 + w/2, 0, d/2)$ at the resonant frequencies for $0 < \theta < 25°$. Gap width is $w = 5$ nm.

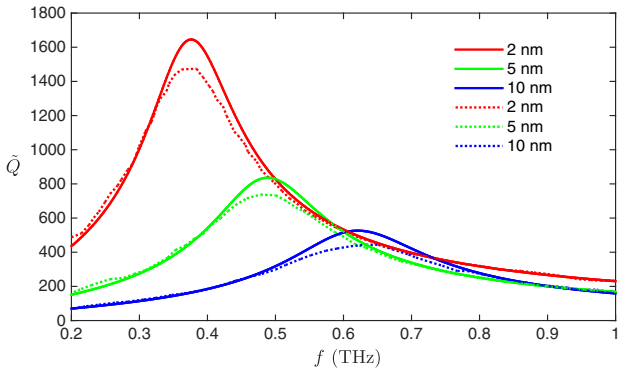

Fig. 15. Field enhancement factor $\tilde{Q}$ obtained by the VMEM method for a single annular gap (solid lines) and by the HDG method for a periodic array of annular gaps (dotted lines).

discontinuous Galerkin (HDG) method, which is an advanced FEM method that is more efficient than the FDTD method or the standard FEM for solving Maxwell's equations [30]. The dotted lines in Fig. 15 show the calculated field enhancement factor $\tilde{Q}$ for the gap width $w = 2$ nm, 5 nm, and 10 nm with the HDG method (cf. [12]). Here the field enhancement factor $\tilde{Q}$ is defined as

$$\tilde{Q} := \int_{S_w} \frac{|E_x|}{|E_x^i|}\mathrm{d}x\mathrm{d}y = \frac{\int_{S_w}|E_x|\mathrm{d}x\mathrm{d}y}{|S_w|\cdot|E_x^i|}.$$

S_w denotes one annulus at the interface between the gap and the vacuum, and $|S_w|$ denotes its area. From the peaks of the field enhancement, it is inferred that the resonant frequencies for three gap sizes are about 0.375 THz, 0.491 THz, and 0.634 THz, respectively.

We apply the VMEM method to simulate the nanostructure with only a single annular gap perforated in the metal film of the same thickness. The diameter of the inner radius is also set as 32 μm. The refractive index of the aluminum is set as 1.73, 2.12, and 2.35 when the gap width $w = 2$ nm, 5 nm, and 10 nm, respectively [31]. The calculated field enhancement factor $\tilde{Q}$ is shown in Fig. 15 (solid lines), and the resonant frequencies for three gap sizes are about 0.376 THz, 0.488 THz, and 0.621 THz, respectively.

We observe that the resonant frequencies obtained for the single gap are very close to the ones obtained for the periodic case, though there exhibit discrepancies in the magnitude of the field enhancement for the two structures. Such deviation may arise from the different nanostructures under consideration. In particular, it should be noted that the scattered field decays in the far-field zone for the single gap structure, while the scattered field for the periodic structure does not decay. In terms of computational complexity, the VMEM method applied here is an inexpensive scheme that involves the solution of the linear system Eq. (14), whereas the HDG method requires decomposing the computational domain with a 3D mesh and solving the linear system obtained from the Galerkin discretization. For instance, when the gap width is 10 nm, the degree of freedom for the VMEM method is only 2672, while the degree for freedom for the HDG method is over 1 million. Note that the FDTD and the standard FEM methods are even more expensive than the HDG method.

5. CONCLUSION

We investigated numerically the extraordinary optical transmission and field enhancement for an annular nanogap perforated in the gold film. Especially, we studied how the resonant frequency, the optical transmission, and the field enhancement depend on the geometric parameters of the gap, the incident angle, and the polarization of the incident wave. The numerical studies provide useful guidance in developing more accurate theoretical models for the scattering problem. It is also useful in providing guidance for the experimental design of nanostructures for specific applications. The VMEM method employed here is very efficient for solving scattering problems with extreme scale difference between the wavelength and the width of the nanogap, which are extremely challenging to solve with conventional FDTD or FEM tools. In particular, it is capable of dealing with the nanostructure with single-digit-nanometer gaps in the terahertz regime without requiring too many computational resources.

Funding. National Science Foundation (NSF) (DMS-1417676, DMS-1719851, NSF ECCS No. 1610333); Research Grants Council of Hong Kong Special Administrative Region, China (CityU 11301914); Fundamental Research Funds for Central Universities of China (2015B19614).

REFERENCES

1. T. W. Ebbesen, H. J. Lezec, H. F. Ghaemi, T. Thio, and P. A. Wolff, "Extraordinary optical transmission through sub-wavelength hole arrays," Nature **391**, 667–669 (1998).
2. F. J. Garcia de Abajo, "Colloquium: light scattering by particle and hole arrays," Rev. Mod. Phys. **79**, 1267–1290 (2007).
3. F. J. Garcia-Vidal, L. Martin-Moreno, T. W. Ebbesen, and L. Kuipers, "Light passing through subwavelength apertures," Rev. Mod. Phys. **82**, 729–787 (2010).
4. D. Mittleman, "Frontiers in terahertz sources and plasmonics," Nat. Photonics **7**, 666–669 (2013).
5. T. Low and P. Avouris, "Graphene plasmonics for terahertz to mid-infrared applications," ACS Nano **8**, 1086–1101 (2014).
6. S. Maier, S. Andrews, L. Martin-Moreno, and F. J. Garcia-Vidal, "Terahertz surface plasmon-polariton propagation and focusing on periodically corrugated metal wires," Phys. Rev. Lett. **97**, 176805 (2006).
7. M. A. Seo, H. R. Park, S. M. Koo, D. J. Park, J. H. Kang, O. K. Suwal, S. S. Choi, P. C. M. Planken, G. S. Park, N. K. Park, Q. H. Park, and D. S. Kim, "Terahertz field enhancement by a metallic nano slit operating beyond the skin-depth limit," Nat. Photonics **3**, 152–156 (2009).
8. X. Chen, H. R. Park, M. Pelton, X. Piao, N. C. Lindquist, H. Im, Y. J. Kim, J. S. Ahn, K. J. Ahn, N. Park, D. S. Kim, and S. H. Oh, "Atomic layer lithography of wafer-scale nanogap arrays for extreme confinement of electro-magnetic waves," Nat. Commun. **4**, 2361 (2013).
9. F. Baida and D. Van Labeke, "Three-dimensional structures for enhanced transmission through a metallic film: annular aperture arrays," Phys. Rev. B **67**, 155314 (2003).
10. W. Gao, J. Shu, K. Reichel, D. V. Nickel, X. He, G. Shi, R. Vajtai, P. M. Ajayan, and J. Kono, "High-contrast terahertz wave modulation by gated graphene enhanced by extraordinary transmission through ring apertures," Nano Lett. **14**, 1242–1248 (2014).
11. M. Haftel, C. Schlockermann, and G. Blumberg, "Enhanced transmission with coaxial nanoapertures: role of cylindrical surface plasmons," Phy. Rev. B **74**, 235405 (2006).

12. H. R. Park, X. Chen, N. C. Nguyen, J. Peraire, and S. H. Oh, "Nanogap-enhanced terahertz sensing of 1-nm-thick (λ/1000000) dielectric films," ACS Photon. **2**, 417–424 (2015).
13. J. Shu, C. Qiu, V. Astley, D. Nickel, D. M. Mittleman, and Q. Xu, "High-contrast terahertz modulator based on extraordinary transmission through a ring aperture," Opt. Express **19**, 26666–26671 (2011).
14. D. Yoo, N. C. Nguyen, L. Martin-Moreno, D. A. Mohr, S. Carretero-Palacios, J. Shaver, J. Peraire, T. W. Ebbesen, and S. H. Oh, "High-throughput fabrication of resonant metamaterials with ultrasmall coaxial apertures via atomic layer lithography," Nano Lett. **16**, 2040–2046 (2016).
15. F. Baida, A. Belkhir, D. Van Labeke, and O. Lamrous, "Subwavelength metallic coaxial waveguides in the optical range: role of the plasmonic modes," Phys. Rev. B **74**, 205419 (2006).
16. P. B. Catrysse and S. Fan, "Understanding the dispersion of coaxial plasmonic structures through a connection with the planar metal-insulator-metal geometry," Appl. Phys. Lett. **94**, 231111 (2009).
17. R. De Waele, S. P. Burgos, A. Polman, and H. A. Atwater, "Plasmon dispersion in coaxial waveguides from single-cavity optical transmission measurements," Nano Lett. **9**, 2832–2837 (2009).
18. D. Li and R. Gordon, "Electromagnetic transmission resonances for a single annular aperture in a metal plate," Phys. Rev. A **82**, 041801 (2010).
19. R. Harrington, *Time-Harmonic Electromagnetic Fields* (Wiley, 2001).
20. X. Lu, H. Shi, and Y. Y. Lu, "Vertical mode expansion method for transmission of light through a single circular hole in a slab," J. Opt. Soc. Am. A **31**, 293–300 (2014).
21. L. Yuan and Y. Y. Lu, "Dirichlet-to-Neumann map method for analyzing hole arrays in a slab," J. Opt. Soc. Am. B **27**, 2568–2579 (2010).
22. L. Yuan and Y. Y. Lu, "An efficient numerical method for analyzing photonic crystal slab waveguides," J. Opt. Soc. Am. B **28**, 2265–2270 (2011).
23. X. Lu and Y. Y. Lu, "Analyzing bull's eye structures by a vertical mode expansion method with rotational symmetry," J. Opt. Soc. Am. B **32**, 2294–2298 (2015).
24. X. Chen, H. R. Park, N. C. Lindquist, J. Shaver, M. Pelton, and S. H. Oh, "Squeezing millimeter waves through a single, nanometer-wide, centimeter-long slit," Sci. Rep. **4**, 6722 (2014).
25. M. A. Ordal, L. L. Long, R. J. Bell, S. E. Bell, R. R. Bell, R. W. Alexander, and C. A. Ward, "Optical properties of the metals Al, Co, Cu, Au, Fe, Pb, Ni, Pd, Pt, Ag, Ti and W in the infrared and far infrared," Appl. Opt. **22**, 1099–1119 (1983).
26. M. Groner, J. W. Elam, F. H. Fabreguette, and S. M. George, "Electrical characterization of thin Al_2O_3 films grown by atomic layer deposition on silicon and various metal substrates," Thin Solid Films **413**, 186–197 (2002).
27. J. P. Berenger, "A perfectly matched layer for the absorption of electromagnetic waves," J. Comput. Phys. **114**, 185–200 (1994).
28. C. Ciraci, R. T. Hill, J. J. Mock, Y. Urzhumov, A. I. Fernndez-Domnguez, S. A. Maier, J. B. Pendry, A. Chilkoti, and D. R. Smith, "Probing the ultimate limits of plasmonic enhancement," Science **337**, 1072–1074 (2012).
29. F. Baida and D. Van Labeke, "Light transmission by subwavelength annular aperture arrays in metallic films," Opt. Commun. **209**, 17–22 (2002).
30. N. C. Nguyen, J. Peraire, and B. Cockburn, "High-order implicit hybridizable discontinuous Galerkin methods for acoustics and elastodynamics," J. Comput. Phys. **230**, 3695–3718 (2011).
31. M. Bareiss, A. Hochmeister, G. Jegert, U. Zschieschang, H. Klauk, R. Huber, D. Grundler, W. Porod, B. Fabel, G. Scarpa, and P. Lugli, "Printed array of thin-dielectric metal-oxide-metal (MOM) tunneling diodes," J. Appl. Phys. **110**, 044316 (2011).